Since January 2020 Elsevier has created a COVID-19 resource centre with free information in English and Mandarin on the novel coronavirus COVID-19. The COVID-19 resource centre is hosted on Elsevier Connect, the company's public news and information website.

Biomaterials 275 (2021) 120986

Contents lists available at ScienceDirect

Biomaterials

journal homepage: www.elsevier.com/locate/biomaterials

A bilirubin-derived nanomedicine attenuates the pathological cascade of pulmonary fibrosis

Hyeongseop Keum [a,b], Dohyeon Kim [a,b], Jinjoo Kim [a,b,1], Tae Woo Kim [a,b], Chang-Hee Whang [a,b], Wonsik Jung [a,b], Sangyong Jon [a,b,*]

[a] Department of Biological Sciences, KAIST Institute for the BioCentury, Korea Advanced Institute of Science and Technology (KAIST), 291 Daehak-ro, Daejeon, 34141, Republic of Korea

[b] Center for Precision Bio-Nanomedicine, Korea Advanced Institute of Science and Technology (KAIST), 291 Daehak-ro, Daejeon, 34141, Republic of Korea

ARTICLE INFO

Keywords:
Antioxidants
Bilirubin
Bilirubin nanoparticles
Nanomedicine
Pulmonary fibrosis
SARS-CoV-2

ABSTRACT

Pulmonary fibrosis is an irreparable and life-threatening disease with only limited therapeutic options. The recent outbreak of COVID-19 has caused a sharp rise in the incidence of pulmonary fibrosis owing to SARS-CoV-2 infection-mediated acute respiratory distress syndrome (ARDS). The considerable oxidative damage caused by locally infiltrated immune cells plays a crucial role in ARDS, suggesting the potential use of antioxidative therapeutics. Here, we report the therapeutic potential of nanoparticles derived from the endogenous antioxidant and anti-inflammatory bile acid, bilirubin (BRNPs), in treating pulmonary fibrosis in a bleomycin-induced mouse model of the disease. Our results demonstrate that BRNPs can effectively reduce clinical signs in mice, as shown by histological, disease index evaluations, and detection of biomarkers. Our findings suggest that BRNPs, with their potent antioxidant and anti-inflammatory effects, long blood circulation half-life, and preferential accumulation at the inflamed site, are potentially a viable clinical option for preventing Covid-19 infection-associated pulmonary fibrosis.

1. Introduction

Pulmonary fibrosis, typically characterized by progressive scarring of the lung parenchyma following lung injury, is considered an intractable and life-threatening disease, usually with a poor prognosis. Because of the numerous risk factors that contribute to its associated lung parenchyma injury, pulmonary fibrosis is often considered an idiopathic disease [1–3]. Notably, recent clinical findings from the COVID-19 pandemic suggest that patients can develop pulmonary fibrosis as sequelae of SARS-CoV-2 infection-induced ARDS that is accompanied by a significant elevation in reactive oxygen species (ROS) levels, resulting in oxidative damage to alveolar epithelial cells (AECs) [4,5]. Subsequently, chemoattractants released from damaged AECs recruit immune cells, especially neutrophils, to the inflamed site. Recruited neutrophils produce additional excess ROS, further exacerbating the redox imbalance and thereby inducing hyper-activation of macrophages as well as terminal differentiation of resident epithelial cells and fibroblasts to myofibroblasts, which secrete autocrine pro-fibrotic mediators, resulting in the exaggerated accumulation of extracellular matrix (ECM) components and lung fibrosis development [6–8]. Hence, the use of potent antioxidant and anti-inflammatory therapeutics that can mitigate excessive oxidative damage in the lung, and thereby prevent further development of pulmonary fibrosis, has been suggested for patients with SARS-CoV-2 infection [9,10].

We recently demonstrated that bilirubin nanoparticles (BRNPs), comprising the potent endogenous antioxidant molecule, bilirubin, exert significant anti-inflammatory efficacy against various oxidative stress-associated diseases, including inflammatory bowel disease (IBD), hepatic ischemia-reperfusion injury (IRI), allergic lung inflammation, islet xenotransplantation, psoriasis, and experimental autoimmune encephalomyelitis (EAE), by effectively scavenging excess ROS upon an inflammatory trigger [11–16]. Encouraged by these previous studies, we hypothesized that BRNPs could successfully reduce exaggerated ROS levels following lung parenchyma injury and hinder propagation of the

* Corresponding author. Department of Biological Sciences, KAIST Institute for the BioCentury, Korea Advanced Institute of Science and Technology (KAIST) , 291 Daehak-ro, Daejeon, 34141, Republic of Korea.

E-mail addresses: hkeum88@kaist.ac.kr (H. Keum), popokyky@kaist.ac.kr (D. Kim), jinjoo21kr@kaist.ac.kr (J. Kim), twkim@kaist.ac.kr (T.W. Kim), cwhang@kaist.ac.kr (C.-H. Whang), jwsik94@kaist.ac.kr (W. Jung), syjon@kaist.ac.kr (S. Jon).

[1] Current affiliation: Clinical Science Team 2, Hanmi Pharm. Co. Ltd., 14 Hanmi tower, Songpa-gu, Seoul 05545, Republic of Korea.

https://doi.org/10.1016/j.biomaterials.2021.120986
Received 30 March 2021; Received in revised form 10 June 2021; Accepted 20 June 2021
Available online 22 June 2021

pathogenic cascade. In the present study, we examine the mechanism by which BRNPs attenuate the pathological cascade of pulmonary fibrosis and exert therapeutic efficacy in a murine bleomycin-induced pulmonary fibrosis model.

2. Materials and methods

2.1. Cell line and culture

The MLE12 mouse lung epithelial cell line was purchased from American Type Culture Collection (ATCC; Manassas, VA, USA) and cultured in Dulbecco's modified Eagle medium (DMEM; Gibco, Grand Island, NY, USA) supplemented with 10% fetal bovine serum (FBS; Gibco) and 1% penicillin/streptomycin (ThermoFisher Scientific, Waltham, MA, USA) at 37 °C in a humidified 5% CO_2 atmosphere.

2.2. Animals

Six-week-old male C57BL/6 wild-type mice were purchased from Orient Bio Inc. Mice were acclimated in a pathogen-free animal facility for 7 d followed by random assignment to groups for further experiments. All animal studies were performed following the NIH Guide for the Care and Use of Laboratory Animals (National Academies Press, 2011), and all animal experimental protocols were approved by the Institutional Animal Care and Use Committee of the Korea Advanced Institute of Science and Technology (KAIST) (IACUC approval number: KA2020-47).

2.3. Synthesis of PEG-BR and preparation of BRNPs

PEGylated bilirubin (PEG-BR) was synthesized as previously described [15]. Briefly, bilirubin (BR) was purchased from Tokyo Chemical Industry, Co. (Tokyo, Japan) and amine-functionalized methoxy-poly(ethylene)glycol ($mPEG_{2K}$–NH_2; Mw ~2000) was purchased from NANOCS (New York, NY, USA). CDI (carbonyldiimidazole; Eq. 1.5; Sigma-Aldrich), dissolved in 2 mL of DMSO (anhydrous dimethyl sulfoxide; Sigma-Aldrich, St. Louis, MO, USA), was added dropwise to bilirubin (BR; Eq.1.0), dissolved in DMSO. After allowing the mixture to react for 1 h, $mPEG_{2K}$–NH_2 (Eq.0.4) was added and allowed to react for an additional 4 h at room temperature (RT). Unreacted BR was then removed by first dissolving in a 5% Na_2CO_3 (200 mL) solution, yielding a bright red product, followed by extraction and purification with chloroform and brine using a separator funnel. The final PEG-BR product (~40% yield) was concentrated *in vacuo* for subsequent characterization by thin-layer chromatography (TLC), ^1H NMR (300 MHz; Bruker, Billerica, MA, USA), and MALDI-TOF/MS (Autoflex 3; Bruker). BRNPs were prepared by dissolving PEG-BR in chloroform, drying under a stream of nitrogen gas, and then further drying under a vacuum, yielding a dark brown film layer. For the formulation of nanoparticles, 500 μl of phosphate-buffered saline (PBS; 137 mM NaCl, 2.7 mM KCl, 10 mM Na_2HPO_4, 2 mM KH_2PO_4) was added to the film layer, and the resulting suspension was sonicated for 10 min, yielding BRNPs dispersed in solution. The resulting orange-brown solution was characterized by TEM (JEOL Ltd., Tokyo, Japan) and DLS (Nanosizer ZS90; Malvern Instruments, Ltd. Malvern, UK).

2.4. In vitro cellular uptake and quantification

In vitro cellular uptake of BRNPs was determined by confocal microscopy imaging and FACS analysis. For cellular uptake examinations, BRNPs were loaded with the fluorescent dye, indocyanine green (ICG). A film layer of PEG-BR was hydrated with a 1-mg/mL aqueous solution of ICG (I2633-25 MG; Sigma-Aldrich), followed by sonication for 15 min in dark, yielding ICG@BRNPs. Free ICG was removed by Sephadex gel filtration and fractionation. The amount of ICG in fraction #3 (~49.13 μg/mL) was the highest, based on a standard curve; accordingly, an equal concentration of free ICG was prepared for quantification of cell uptake. For confocal imaging, MLE12 cells were seeded on sterile coverslips in a 12-well plate at a density of 3×10^5 cells/well. After incubating overnight, the cells were incubated with PBS, free ICG, or an equivalent amount of ICG@BRNPs for 4 h. The samples were washed twice with 1x PBS, fixed with 1% paraformaldehyde (Sigma-Aldrich), and stained with Hoechst 33,342 (ThermoFisher Scientific) for 10 min to stain nuclei. The samples were mounted on glass slides (Marienfeld Superior, Lauda-Konigshofen, Germany), covered with mounting medium (Dako, Carpinteria, CA, USA), and analyzed using a confocal microscope (LSM 780; Carl Zeiss Inc., Oberkochen, Germany). For FACS experiments, MLE12 cells were seeded in a 6-well plate at a density of 5×10^5 cells/well and incubated overnight. Sample preparation was as described for confocal imaging analysis except that nuclear staining was omitted. The collected cells were analyzed using a LSR Fortessa high-performance multi-parameter flow cytometer (BD Bioscience, San Jose, CA, USA), processed with FlowJo software (Tree Star Inc., San Carlos, CA, USA).

2.5. Cell viability and in vitro cytoprotective test

Cell viability was examined using a WST-8 cell viability assay kit (Biomax, Seoul, Korea) following the manufacturer's instructions. MLE12 cells were seeded in a 96-well plate at a density of 5×10^3 cells/well. After incubating overnight, the cells were incubated with different concentrations of BRNPs (5–1000 μg/mL) for 24 h. The WST-8 reagent (10 μL/well) was then added and plates were incubated in a 37 °C incubator for up to 2 h, after which absorbance at 450 nm was measured using a VersaMax microplate reader (Molecular Devices, Sunnyvale, CA, USA). For the cytoprotective test, MLE12 cells were seeded at a density of 5×10^3 cells/well in a 96-well plate and allowed to stabilize overnight. Cells were then treated with different concentrations (5–1000 μg/mL) of BRNPs for 4 h, followed by washing with PBS to remove any BRNPs that had not been taken up. Thereafter, MLE12 cells were exposed to oxidative stress by incubating with 200 μM H_2O_2 for 24 h. After incubation, the viability of the cells was assessed using a WST-8 cell viability kit. For the ROS assessment, MLE12 cells were treated with 1000 μg/mL of BRNPs for 4 h, followed by washing and addition of H_2O_2 (final concentration: 200 μM) for 24 h. ROS was visualized by staining the cells with 20 μM of 2′-7′-dichlorofluorescein diacetate (DCF-DA) for 30 min at 37 °C in a humidified 5% CO_2 atmosphere. For mitochondria staining, the same protocol from ROS staining was performed except for the staining using a MitoTracker (M7512; ThermoFisher Scientific) according to the manufacturer's instructions. Prepared samples were imaged using a confocal microscope.

2.6. Evaluation of the in vitro cytoprotective effect of BRNPs against bleomycin-induced oxidative damage

For cell viability tests, MLE12 cells were seeded at a density of 5×10^3 cells/well in a 96-well plate and allowed to stabilize overnight. Cells were treated with different concentrations (5–1000 μg/mL) of BRNPs for 2 h, after which bleomycin (100 μg/mL) was added and cells were incubated for 24 h. Cell viability was then assessed using a WST-8 cell viability kit as described above. For apoptosis assessment, MLE12 cells were seeded at a density of 3×10^5 cells/well in a 6-well plate and incubated overnight. Thereafter, cells were treated with 1000 μg/mL of BRNPs for 2 h, followed by exposure to harsher oxidative stress conditions by stimulating with a higher concentration (200 μg/mL) of bleomycin. Thereafter, samples were washed and prepared for flow cytometry-based TUNEL assay using a Click-it Plus TUNEL Assay kit (C10619; Invitrogen, Waltham, MA, USA).

2.7. Relative quantification of apoptosis-associated and chemoattractant gene levels

MLE12 cells were seeded at a density of 3×10^5 cells/well in a 6-well plate and incubated overnight. Cells were pretreated with BRNPs (1000 μg/mL) for 2 h and then stimulated with 100 μg/mL of bleomycin for 24 h. Total RNA from each group was extracted using an RNA extraction kit (GeneAll, Seoul, Korea) following the manufacturer's instructions, and RNA concentration was measured using a NanoDrop 1000 spectrophotometer (ThermoFisher Scientific). RT-PCR analyses were performed on a Rotor-Gene Q Real-Time PCR system (QIAGEN, Germantown, MD, USA) using samples containing equal amounts of RNA, RT-PCR master mix (LeGene Bioscience, San Diego, CA, USA) and the appropriate primers. The following genes were analyzed using the indicated primer pairs: p53, 5′-CGC TGC TCC GAT GGT GAT-3' (forward) and 5′-GGC GAA AAG TCT GCC TGT CTT-3' (reverse); Bax, 5′-GGG TGG CAG CTG ACA TGT TT-3' (forward) and 5′-GCC TTG AGC ACC AGT TTG CT-3' (reverse); Bcl-2, 5′-TGA GTA CCT GAA CCG GCA TCT-3' (forward) and 5′-GCA TCC CAG CCT CCG TTA T-3' (reverse); MCP-1, 5′-TTA AAA ACC TGG ATC GGA ACC AA-3' (forward) and 5′-GCA TTA GCT TCA GAT TTA CGG GT-3' (reverse); CXCL8, 5′-ACT CCC CTT TAC CCA GTG GA-3' (forward) and 5′-GGA CCA TGG CTT GAC CAT CA-3' (reverse).

2.8. Bleomycin-induced pulmonary fibrosis animal model and treatment

The mouse pulmonary fibrosis model was created with a single lung administration of bleomycin (bleomycin sulfate; Tokyo Chemical Industry Co.) dissolved in 1x PBS. Each mouse received a weight-adjusted 1.5-mg/kg dose of bleomycin via oropharyngeal aspiration. Before administration, mice were anesthetized with 30 mg/kg of tiletamine/zolazepam and 10 mg/kg of xylazine. Mice in the control group received an equal volume (50 μL) of saline. During administration, the mouse's nostril was occluded with a thumb, forcing the mouse to breathe through its mouth and thus enhancing deposition into the lung. The thumb was released after the completion of five breaths. The UCB solution for intravenous injection was prepared by fully dissolving bilirubin in NaOH solution, followed by adjusting the solution pH to ~7–8 using an HCl solution. Starting on day 1, 50 μL of saline or UCB (4.64 mg/kg) or BRNPs (5, 20, 40 mg/kg) were intravenously injected via the retro-orbital route every other day for 14 days.

2.9. Biodistribution, cellular uptake, and ROS analyses followed by systemic injection of BRNPs in a pulmonary fibrosis animal model

Pulmonary fibrosis mice, prepared as described above, were treated 14 days after the bleomycin challenge with free cypate (dissolved in 5% DMSO) or an equal dose of cypate-loaded BRNPs (cypate@BRNPs) via retro-orbital injection. cypate@BRNPs were prepared by rehydrating a film layer of PEG-BR and cypate mixture (1:2, w/w) in chloroform with distilled water, followed by sonication for 15 min. Unencapsulated cypate in the resulting solution was removed by gel filtration and subsequent fractionation. The *ex vivo* biodistribution of cypate@BRNPs in isolated major organs (liver, heart, lung, kidney, spleen, intestine) was examined 6 h after injection using an IVIS Spectrum *in vivo* Imaging System (PerkinElmer, Waltham. MA, USA). For analysis of the cell-specific uptake of BRNPs, cypate@BRNPs were intravenously injected on day 7 of the bleomycin challenge. The whole lung tissue was homogenized using a lung disassociation kit (130-095-927; Miltenyi Biotec, Bergisch Gladbach, North Rhine-Westphalia, Germany) 4 h after injection. The cell pellet was incubated with RBC hemolysis buffer (Sigma-Aldrich) for 5 min and centrifuged for 5 min at 4 °C. Collected primary lung cells were stained with a fixable viability dye, eFluor 506 (65-0866-14; eBioscience, ThermoFisher Scientific), allophycocyanin (APC)-conjugated anti-CD11b (17-0112-81; eBioscience), Qdot605-conjugated anti-Gr-1 (RB6-8C5; BD Biosciences), eFluor 450-conjugated anti-F4/80 (48-4801-82; eBioscience), fluorescein isothiocyanate (FITC)-conjugated anti-EPCAM (11-5791-82; eBioscience), PE-conjugated anti-ER-TR7 (sc-73355; Santa Cruz Biotechnology, Dallas, USA) (0.25 μg/sample). Cells were then washed again with two changes of 1x PBS, and the final samples for following flow cytometry analyses were prepared by adding fresh 1x PBS. For measuring ROS levels within primary lung cells, on day 1, 50 μL of saline or BRNPs (20 mg/kg) were intravenously administered to bleomycin-induced pulmonary fibrosis mice every other day. On day 7, the mice were euthanized and retrieved lung tissues were homogenized using a lung dissociation kit. The isolated primary lung cells were treated with 20 μM of DCF-DA for 30 min at 37 °C in a humidified 5% CO_2 atmosphere. After incubation, the samples were carefully washed and the pellets were resuspended in a fresh 1x PBS. The resulting samples were analyzed using a LSR Fortessa high-performance multi-parameter flow cytometer and processed with FlowJo software.

2.10. Analysis of pulmonary fibrosis indexes

Bodyweight was measured daily prior to administration of BRNPs or saline to avoid biasing body weight results. Upon sacrifice, the weights of intact lungs were measured. Then, wet weights of left-side lung samples were measured, and the same samples were completely dried using a freeze-drying vacuum. Fully dehydrated lung samples were collected, and their weights were measured.

2.11. Preparation and histological analysis of lung tissues

Right lung samples were immediately washed with 1x PBS, fixed by incubating with 4% paraformaldehyde for 12 h, dehydrated, processed into paraffin blocks, and sectioned (4 μm thickness) onto HistoBond glass slides (Marienfeld Superior) using a CM 1850 microtome (Leica, Wetzlar, Germany). Prepared tissue samples were deparaffinized using histological grade xylene (Sigma-Aldrich) and rehydrated for H&E and MT staining. Stained samples were washed three times with distilled water to remove excess dye, followed by serial dehydration with two changes of 95% ethanol and 100% ethanol. The stained tissues were cleared with two changes of xylene (3 min each) and mounted with Permount mounting medium (Fisher Scientific). The histology of mounted lung samples was visualized using an inverted microscope (Eclipse Ti2; Nikon, Tokyo, Japan). Pulmonary fibrosis scores for lung samples were calculated using an objective Ashcroft scoring system, performed by a third party blinded to group-identifying information. The fibrotic fraction was quantified using ImageJ software, version 1.49 (NIH).

2.12. BALF collection and sample preparation

The trachea was exposed by making a small neck incision, after which the mouse was cannulated intratracheally with a 20-gauge polyurethane catheter (BRAUN, Hessen, Germany). Cold PBS (1 mL) was injected into the lungs and recovered three times, yielding a total of 3 mL BALF. BALF cells were isolated by centrifugation (1350 rpm, 10 min, 4 °C), and the protein-containing supernatant was collected and kept at −80 °C for further analysis. The cell pellet was incubated with RBC hemolysis buffer for 5 min and centrifuged. Prepared cells were stained with the fixable viability dye, eFluor 506 (65-0866-14; eBioscience), followed by immunostaining with following antibodies for 60 min at 4 °C in the dark: FITC-conjugated anti-CD11b (11-0112-82; eBioscience), Qdot605-conjugated anti-Gr-1 (RB6-8C5; BD Biosciences), eFluor 450-conjugated anti-F4/80 (48-4801-82; eBioscience), phycoerythrin (PE)-cyanine 5-conjugated CD80 (15-0801-82; eBioscience), and PE-cyanine 7-conjugated CD86 (25-0862-82; eBioscience) (0.25 μg/sample). Cells were then washed again with two changes of 1x PBS, and the final samples were prepared by adding fresh PBS containing 1% paraformaldehyde. Samples were analyzed using an LSR Fortessa high-performance multi-parameter flow cytometer, processed with FlowJo

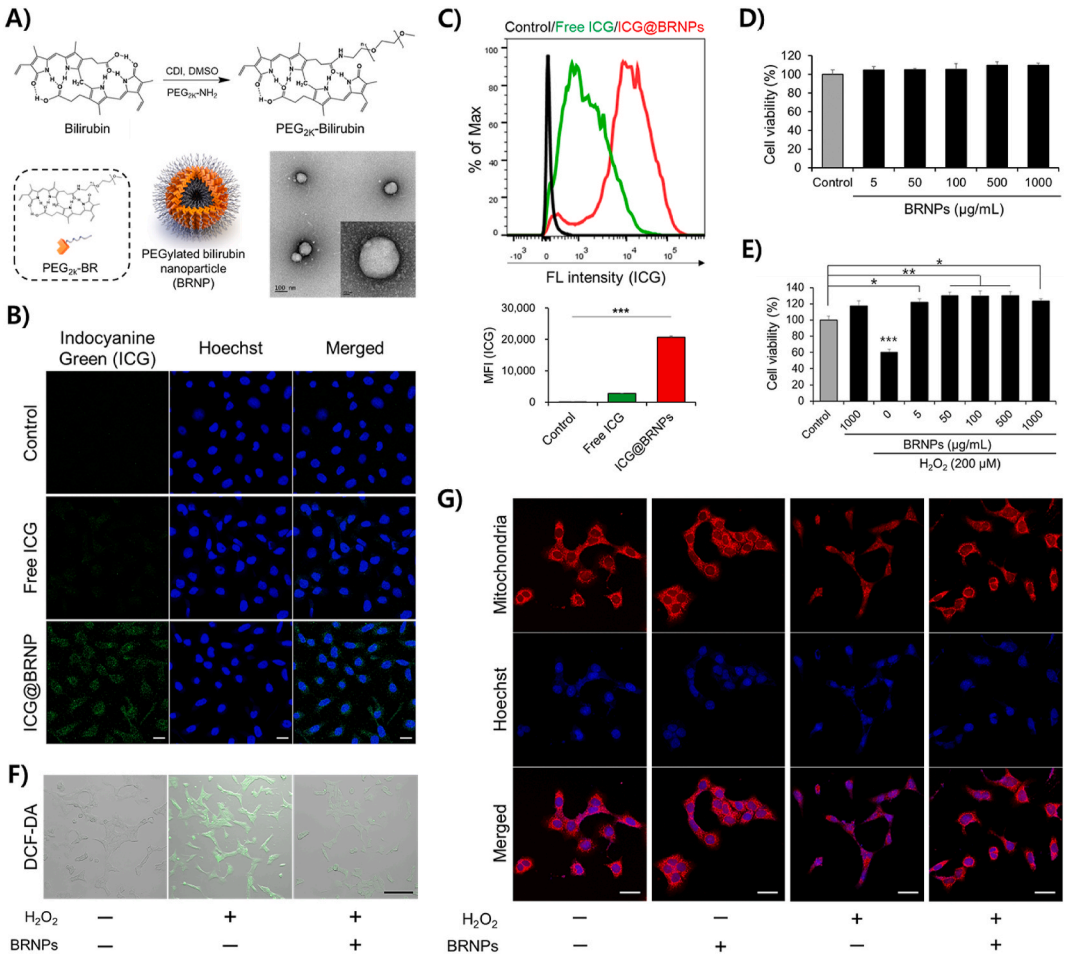

Fig. 1. BRNPs are readily taken up by lung epithelial cells (MLE12) and protect the cells from oxidative stress by scavenging cellular oxidative molecules. (A) Synthetic scheme for PEG-BR. BRNPs were generated with a film layer/rehydration method using PEG-BR, as shown in TEM images. Scale bars, 100 nm (inset: 20 nm). (B) Cellular uptake of BRNPs in MLE12 cells was analyzed by confocal microscopy and (C) flow cytometry using indocyanine green (ICG)-loaded BRNPs. Scale bars, 20 μm. (D) The viability of MLE12 lung epithelial cells was assessed after treatment for 24 h with different concentrations (5–1000 μg/mL) of BRNPs. (E) BRNPs protected MLE12 cells from oxidative stress induced by H_2O_2. Cells were pre-treated with BRNPs for 2 h and then incubated with H_2O_2 for an additional 24 h. (F) Intracellular ROS generation in H_2O_2-stimulated MLE12 cells treated with BRNPs under different conditions was visualized using DCF-DA, a ROS-responsive fluorescent indicator. Scale bars, 100 μm. (G) Representative staining of mitochondria in MLE12 cells under different treatment conditions (H_2O_2, 200 μM; BRNPs, 1000 μg/mL). Scale bars, 20 μm. Data are presented as means ± standard error of the mean (SEM). Statistical analyses were performed using a one-way analysis of variance (ANOVA) followed by Tukey's post hoc tests for comparison of differences between two groups. *P*-values < 0.05 were considered statistically significant; individual *P*-values are indicated by asterisks in figures (***$P < 0.001$, **$P < 0.01$, *$P < 0.05$). DCF-DA, 2′-7′-dichlorofluorescein diacetate. (For interpretation of the references to color in this figure legend, the reader is referred to the Web version of this article.)

software. The preserved BALF supernatant was used for quantifying the following cytokines using ELISA kits: IL-6 (DY406-05; R&D Systems, Minneapolis, MN, USA), TNF-α (DY410-05; R&D Systems), IL-10 (DY417-05; R&D Systems), and TGF-β (DY1679-05; R&D Systems). ELISAs were performing according to the manufacturer's recommendations.

2.13. Lung homogenization and sample preparation

Collected lung tissue was homogenized using a lung dissociation kit and incubated with RBC hemolysis buffer for 5 min and centrifuged for collection (1350 rpm for 5 min at 4 °C). Prepared cells were stained with the fixable viability dye, eFluor 506 (65-0866-14; eBioscience), and then immunostained by incubating with the following antibodies for 60 min at 4 °C in the dark: FITC-conjugated anti-EPCAM (11-5791-82; eBioscience), PE-conjugated anti-ER-TR7 (sc-73355; Santa Cruz Biotechnology), and APC-conjugated anti-vimentin (IC2105A; R&D Systems) (0.25 μg/sample). Samples were washed twice with 1x PBS and the final samples were prepared by adding fresh PBS containing 1% paraformaldehyde. Samples were analyzed using a LSR Fortessa high-performance multi-parameter flow cytometer, processed with FlowJo software.

3. Results and discussion

3.1. BRNPs are efficiently taken up by lung epithelial cells and protect cells from oxidative stress

BRNPs were prepared from self-assembly of hydrophilic poly (ethylene glycol)-modified bilirubin (PEG-BR) in an aqueous solution (Fig. 1A) [15]. The size of BRNPs measured by transmission electron microscopy (TEM) (Fig. 1A) and dynamic light scattering (DLS) (Fig. S1A) was approximately 120–140 nm. Zeta potential measurements showed that BRNPs displayed a slightly negative surface charge (Fig. S1B). Using indocyanine green (ICG)-loaded BRNPs (ICG@BRNPs), we first examined whether BRNPs are taken up by the lung epithelial cell line, MLE12 (Fig. S2). Confocal microscopy imaging (Fig. 1B) and flow cytometry (Fig. 1C) experiments revealed that, unlike free ICG dye,

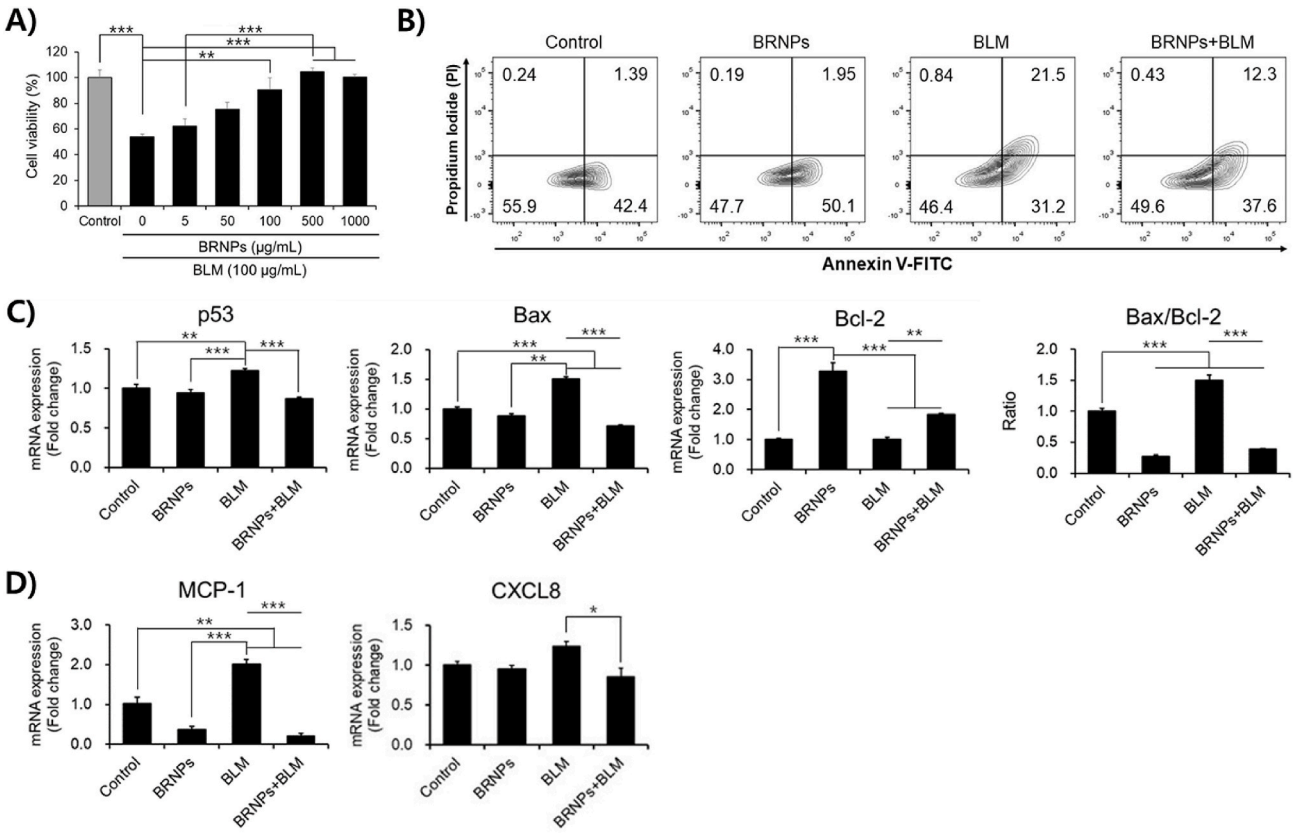

Fig. 2. BRNPs exert anti-apoptotic effects in MLE12 cells, attenuating apoptosis resulting from bleomycin-induced oxidative damage, and sustain upregulation of chemoattractant genes. (A) BRNPs protected MLE12 cells from bleomycin-induced oxidative stress. MLE12 cells were pre-treated with BNRPs (1000 μg/mL) for 2 h, followed by stimulation of oxidative with 100 μg/mL of bleomycin for 24 h. Viability was quantified using a WST-8 cell viability assay kit. (B) Anti-apoptotic effects of BRNPs, analyzed by annexin-V/PI staining. MLE12 cells were pre-treated with BRNPs (1000 μg/mL) for 2 h and then stimulated with bleomycin (200 μg/mL) for 24 h. (C) MLE12 cells were treated with BRNPs (1000 μg/mL) for 2 h, then stimulated with bleomycin (100 μg/mL) for 24 h, after which total RNA was extracted and apoptosis-associated (p53, Bax, and Bcl-2) and (D) chemoattractant (MCP-1 and CXCL8) genes were measured by quantitative RT-PCR. Data are presented as means ± SEM (***$P < 0.001$, **$P < 0.01$, *$P < 0.05$; one-way ANOVA followed by Tukey's post hoc test). BLM, bleomycin treatment.

ICG@BRNPs were readily internalized into MLE12 cells. A subsequent evaluation of the cytotoxicity and cytoprotective efficacy of BRNPs showed that MLE12 cells treated with different concentrations of BRNPs exhibited no changes in viability, suggesting that BRNPs do not exert overt cellular cytotoxicity in these cells (Fig. 1D). Since hydrogen peroxide (H_2O_2) is a representative ROS elevated in oxidative stress-related inflammation, we next treated MLE12 cells with H_2O_2 (200 μM) in the absence or presence of BRNPs. Whereas treatment with H_2O_2 considerably reduced cell viability compared with untreated controls, BRNPs, even at the lowest concentration (5 μg/mL), were able to protect cells from H_2O_2-induced oxidative damage (Fig. 1E). Similarly, the number of MLE12 cells exhibiting high levels of intracellular ROS production, monitored using the ROS-responsive fluorescent indicator, DCF-DA, was substantially increased by stimulation with H_2O_2, whereas ROS-reactive DCF-DA signals were substantially blunted by BRNP treatment (Fig. 1F). Moreover, compared with the control group, the H_2O_2-only treatment group showed obvious mitochondrial fragmentation (Fig. 1G), whereas groups treated with BRNPs, with or without H_2O_2 stimulation, showed no appreciable mitochondrial fragmentation. Collectively, these results clearly indicate that BRNPs are non-toxic and possess highly potent ROS scavenging ability, and are thus capable of protecting lung epithelial cells from oxidative damage.

3.2. BRNPs protect MLE12 cells from bleomycin-induced oxidative damage and suppress upregulation of pro-apoptosis and chemoattractant genes

The use of bleomycin is a well-established method for inducing lung fibrosis in mice. It has been established that bleomycin forms a complex with endogenous ferric iron (Fe^{3+}) and generates reactive oxygen radicals, inducing apoptosis of alveolar epithelial cells and causing lung injury [17]. Given the cytoprotective effect of BRNPs on H_2O_2-treated MLE12 cells (Fig. 1), we examined the effect of BRNPs on bleomycin-treated MLE12 cells. As expected, BRNPs effectively protected MLE12 cells from oxidative damage induced by 100 μg/mL bleomycin (Fig. 2A). Even at a bleomycin concentration as high as 200 μg/mL, BRNP treatment led to a much lower late apoptotic cell population (12.3%) compared with bleomycin-only–treated MLE12 cells (21.5%) (Fig. 2B). Next, the anti-apoptotic effect of BRNPs was evaluated at the gene level by measuring the expression of mitochondrial apoptosis-related genes and monocyte and neutrophil chemoattractant genes by reverse transcription-polymerase chain reaction (RT-PCR) analysis. In keeping with the fact that the p53/Bax/Bcl-2 pathway is a hallmark of apoptotic signaling [18,19], we found that bleomycin treatment induced an increase in the pro-apoptosis genes, p53 (tumor protein p53) and Bax (Bcl-2-associated X protein), an effect that was significantly attenuated by BRNP treatment. Interestingly, expression of the anti-apoptosis gene, Bcl-2, was significantly upregulated by BRNP treatment, suggesting that BRNP may exert an anti-apoptotic effect on cells apart from its ability to scavenge ROS (Fig. 2C). Similarly, BRNP

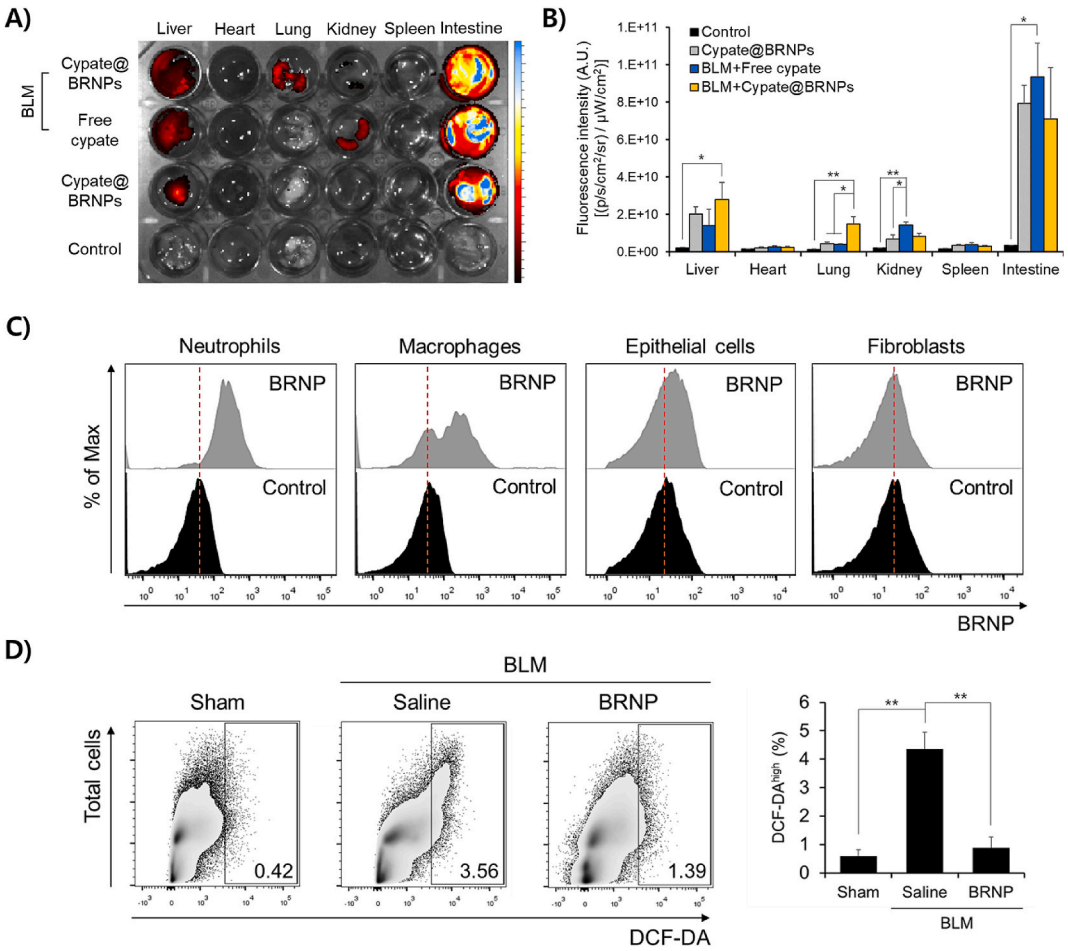

Fig. 3. Systemically administered BRNPs accumulate in the lung, internalize in various cell types, and collectively lower the ROS level of bleomycin-challenged animals. (A) Representative *ex vivo* image of the biodistribution of BRNPs to major organs (liver, heart, lung, kidney, spleen, intestine) after retro-orbital injection of free cypate or cypate-loaded BRNPs (cypate@BRNPs). The image was obtained 6 h post-administration using IVIS. (B) Quantification of fluorescence in dissected major organs 6 h after retro-orbital injection of free cypate or cypate@BRNPs. (C) Flow cytometry data represented in histograms for uptake of cypate@BRNPs by primary lung cells isolated after intravenous injection to bleomycin-induced pulmonary fibrosis mice on day 7. (D) Flow cytometry data represented in dot-plots for cell population of primary lung cells expressing high level of DCF-DA staining. The primary lung cells were isolated after periodical intravenous injection of BRNPs in a bleomycin-induced pulmonary fibrosis model. Data are presented as means ± SEM (**$P < 0.01$, *$P < 0.05$; one-way ANOVA followed by Tukey's post hoc test). BLM, bleomycin-induced pulmonary fibrosis mice.

treatment repressed expression levels of genes encoding chemokines, including monocyte chemoattractant protein-1 (MCP-1) and the neutrophil attractant, CXCL8 (chemokine C-X-C motif ligand 8), which are known to be released following alveolar epithelial cell activation and apoptosis (Fig. 2D) [20–23]. These findings suggest that BRNPs protect MLE12 cells from oxidative damage by downregulating pro-apoptosis and chemoattractant gene expression.

3.3. *BRNPs are distributed in fibrosis-progressive lung tissue, internalized into various cells, and reduce total ROS level in the lung*

We next determined the biodistribution of systemically administered BRNPs in both disease-free and bleomycin-induced pulmonary fibrosis models using BRNPs loaded with the near-infrared dye, cypate (cypate@BRNPs). At 6 h post-injection in a disease-free mouse, cypate@BRNPs appeared to localize primarily in the liver and was excreted into the intestine—a typical enterohepatic metabolic pathway for bilirubin [24,25] (Fig. 3A and B). Interestingly, in mice with bleomycin-induced pulmonary fibrosis, BRNP localization to the lung was significantly increased compared with that in a disease-free mouse, together with a similar large accumulation in the liver and excretion into the intestine; free cypate did not show increased localization in the lung.

We speculate that this enhanced localization of cypate@BRNPs in the inflamed lung reflects the passive entry of long-circulating BRNPs into the lung parenchyma, where leaky blood vessels, formed as a result of locally induced inflammation, allow tissue infiltration of BRNPs [11,26]. Next, we examined cell type-specific uptake of BRNPs in the lung after intravenous injection of cypate@BRNPs. We found that BRNPs were largely taken up by phagocytic cells such as macrophages and neutrophils in the lung and also partially internalized in the lung epithelial cells; however, no signal of BRNP internalization was observed in fibroblasts (Fig. 3C). Furthermore, total ROS level in the isolated primary lung cells from the pulmonary fibrosis-induced mice was significantly reduced by BRNP treatment compared to the saline-treated disease mice as evidenced by DCF-DA staining (Fig. 3D) and associated mean fluorescence intensity (MFI) data (Fig. S3). These findings indicate that BRNPs upon systemic injection can localize at inflamed lung where they are taken up by phagocytic cells and epithelial cells and also scavenge excess ROS that play a crucial role in initiation and propagation of the pathogenic cascade of pulmonary fibrosis.

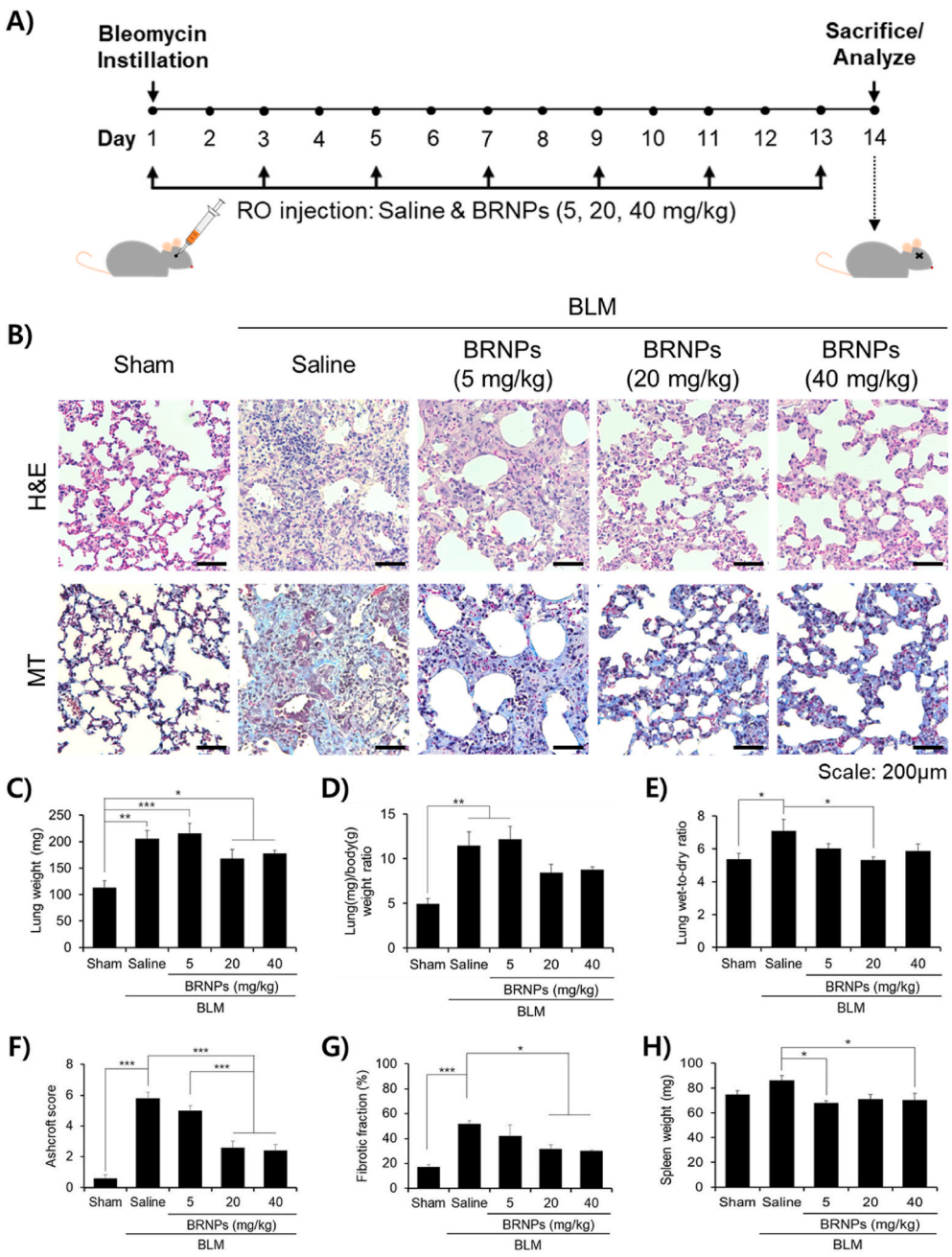

Fig. 4. Intravenous injection of BRNPs alleviates pulmonary fibrosis symptoms. (A) Experimental protocol for the bleomycin-induced pulmonary fibrosis animal model. Pulmonary fibrosis was induced with a single intratracheal instillation of bleomycin (1.5 U/kg). Starting on day 1, different concentrations of BRNPs were intravenously administered every other day for 14 d. (B) Representative histological images of H&E and MT-stained tissue sections from the bleomycin-induced lung fibrosis animal model after treatment with different concentrations of BRNPs. Scale bars, 200 μm. (C–H) Indexes of pulmonary fibrosis. Data are presented as means ± SEM (***P < 0.001, **P < 0.01, *P < 0.05; one-way ANOVA followed by Tukey's post hoc test). IV, Intravenous. BLM, bleomycin-induced pulmonary fibrosis mice.

3.4. *BRNPs mitigate symptoms of pulmonary fibrosis in a bleomycin-induced mouse model*

Having confirmed the potent cytoprotective effect and lung localization of BRNPs, we examined the therapeutic efficacy of BRNPs in a bleomycin-induced pulmonary fibrosis animal model. Mice were intravenously administered with BRNPs at doses of 5, 20, and 40 mg/kg every other day. On day 14, the mice were euthanized and analyzed (Fig. 4A). Pathological signs of pulmonary fibrosis were analyzed by hematoxylin & eosin (H&E) and Masson's trichrome (MT) staining of lung tissue sections. In the saline-treated control group, H&E staining revealed a profound increase in lung tissue density, with particularly thickened alveolar walls and noticeable alteration of lung structures and infiltration of inflammatory cells (Fig. 4B). In contrast, alveolar and bronchiole wall thickening were only moderately increased by both medium- and high-dose BRNP treatment (20 and 40 mg/kg), and the density of lung tissue and infiltrated inflammatory foci were only slightly altered in these groups compared with those in the sham group; H&E staining analyses showed that low-dose BRNP treatment (5 mg/kg) was ineffective. In samples stained with MT, which reacts with collagen to produce a blue color, only a small amount of collagen accumulation was detected in both disease-free and BRNP (20 and 40 mg/kg)-treated groups; in contrast, significant collagen deposition was seen throughout the field in sections from mice treated with saline or 5 mg/kg BRNPs (Fig. 4B). Similar results were observed for bodyweight measurements obtained over the course of the *in vivo* study (Fig. S4). An increase in the lung weight and lung/body (L/B) weight ratio is characteristic of lungs with fibrosis-induced lung damage owing to extravagant ECM buildup [27,28]. Intratracheal instillation of bleomycin (bleomycin + saline treated group) induced a fibrosis-like lung condition, as demonstrated by significant increases in lung weight and L/B weight ratio (Fig. 4C and D). Remarkably, the bleomycin-induced increase in lung weight was diminished in mice co-treated with 20 or 40 mg/kg BRNPs (bleomycin + BRNPs group), and only a slight increase in L/B weight ratio was

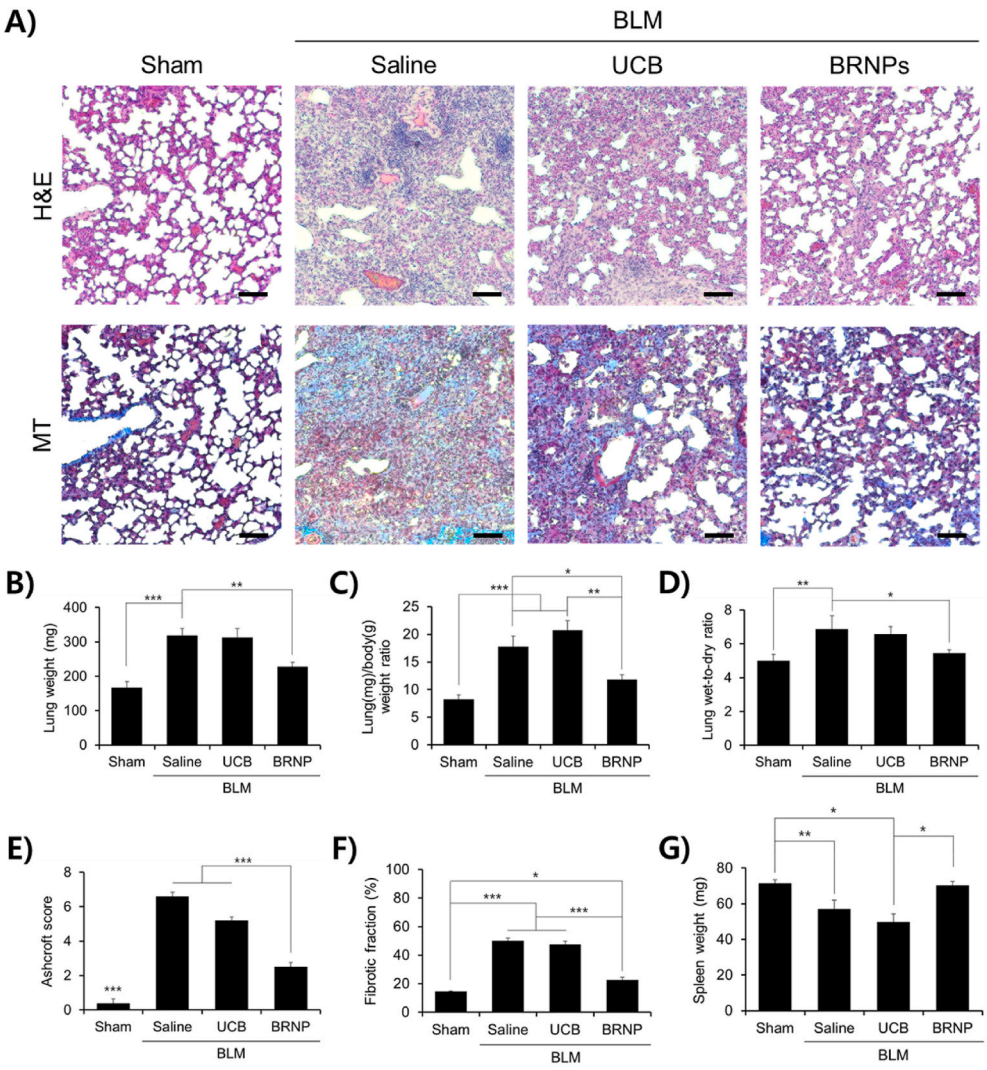

Fig. 5. BRNPs exert a potent therapeutic effect compared with UCB. The effects of BRNPs administration were monitored after treatment with BRNPs (20 mg/kg) or an equivalent dose of UCB (4.64 mg/kg) in a bleomycin-induced lung fibrosis animal model. (A) Representative images of H&E– and MT-stained tissue sections. Scale bars, 200 μm. (B–G) Indexes of pulmonary fibrosis. BLM, bleomycin (1.5 U/kg). Data are presented as means ± SEM (***P < 0.001, **P < 0.01, *P < 0.05; one-way ANOVA followed by Tukey's post hoc test). BLM, bleomycin-induced pulmonary fibrosis mice. UCB, Unconjugated bilirubin.

observed in these mice. We also assessed increases in lung wet-to-dry (W/D) ratio, which is an indicator of potential lung complications, reflecting the fact that lung permeability is dysregulated in damaged lungs, resulting in pulmonary edema (i.e., surplus accumulation of water in the lungs) [29–31]. Whereas mice in the saline-treated group presented with a notable rise in the W/D ratio, mice treated with bleomycin + BRNPs (especially at 20 mg/kg) showed only a negligible escalation in this ratio (Fig. 4E), a finding that is in agreement with lung weight and L/B ratio results. Disease severity was reaffirmed using an objective Ashcroft scoring system (Fig. 4F) and quantification of the fibrotic fraction (Fig. 4G). In this context, administration of bleomycin caused a degree of splenomegaly that was attenuated in mice treated with BRNPs (Fig. 4H), suggesting that BRNP treatment prevents the induction of inflammation. Collectively, these results suggest that administration of BRNPs at 20 or 40 mg/kg is highly effective in ameliorating the symptoms of pulmonary fibrosis; accordingly, a concentration of 20 mg/kg of BRNPs was chosen for subsequent evaluations.

3.5. *BRNPs are more efficient in alleviating pulmonary fibrosis symptoms than unconjugated bilirubin*

Because BRNPs composed of PEGylated bilirubin have a much longer blood circulation time and higher colloidal stability than the hydrophobic small molecule, unconjugated bilirubin (UCB), the former nanomedicine is predicted to exhibit better therapeutic efficacy than the latter [12–14,16]. To test this, we intravenously injected either BRNPs (20 mg/kg; equivalent to 4.64 mg UCB/kg) or an equivalent dose of UCB (4.64 mg/kg) into bleomycin-induced pulmonary fibrosis mice. Because involuntary bodyweight loss is a characteristic symptom of pulmonary fibrosis, whole body weight and survival of bleomycin-challenged mice were monitored daily throughout the 14-day study. Whereas both bleomycin + saline and bleomycin + UCB treatment groups showed a continuous drop in body weight, bleomycin + BRNPs treatment led to the recovery of body weight by the time of euthanization (Fig. S5A). In addition, a survival analysis showed a deteriorating survival rate for the bleomycin + UCB group, whereas all mice in the bleomycin + BRNPs group survived to the study end-point (Fig. S5B). Subsequent histological evaluations supported these phenotypic changes, revealing significantly increased tissue density with notably distorted lung structures, alveolar wall thickening, and collagen deposition in the lung parenchyma of mice in the UCB-treated group, but showing a dramatic decrease in these indications in the BRNP-treated group (Fig. 5A). Similarly, lung weight and L/B weight ratio were significantly increased for bleomycin + saline and bleomycin + UCB treatment groups, indicating the development of lung fibrosis, whereas both indications were attenuated by treatment with BRNPs (Fig. 5B and C). An increased W/D ratio was also observed in saline and UCB-treated groups, but this ratio remained close to that of the normal control group in mice treated with BRNPs (Fig. 5D). Diagnose of disease severity using Ashcroft scores and quantification of the fibrosis-positive fraction (Fig. 5E and F) further

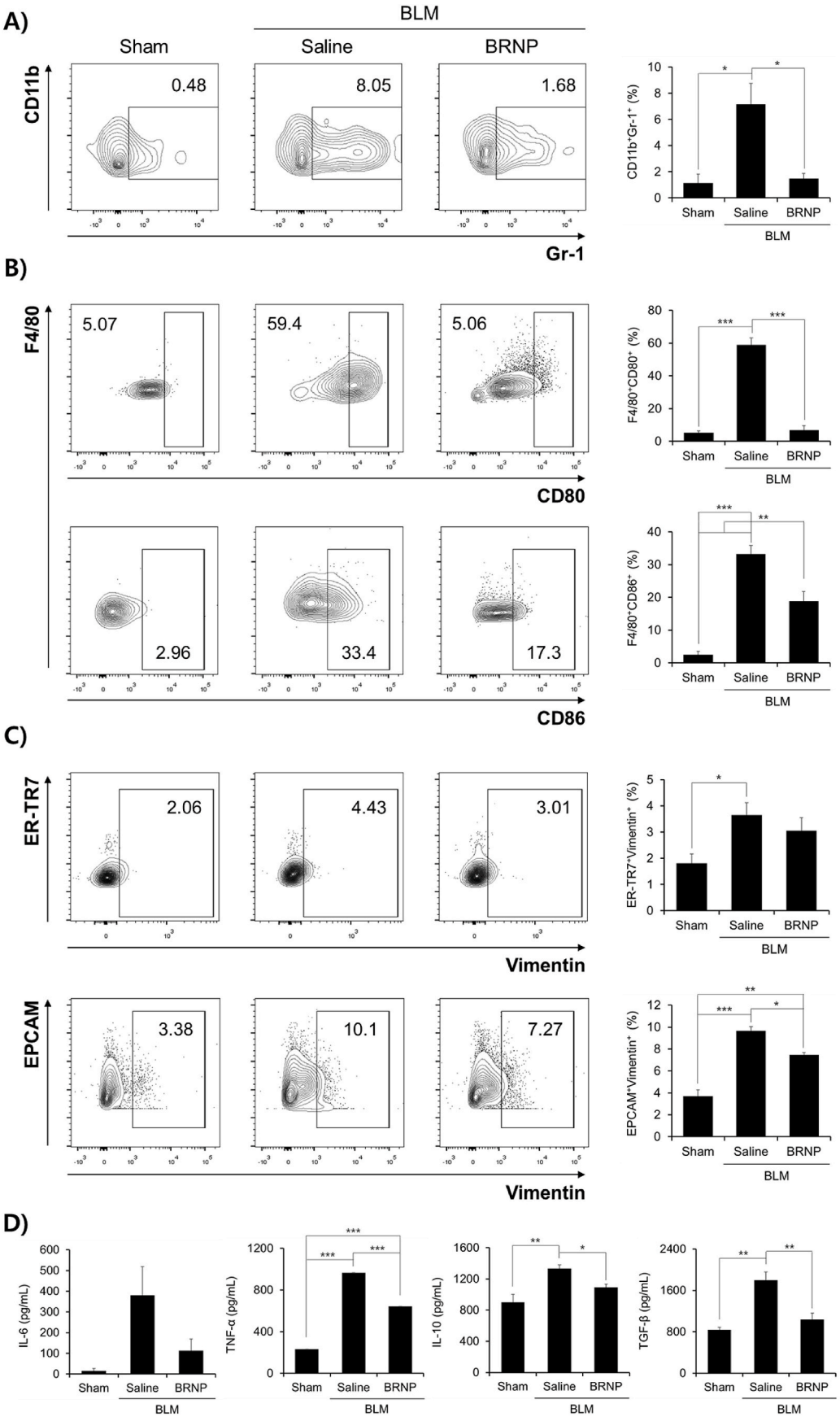

Fig. 6. BRNPs treatment decreases infiltration of neutrophils, suppresses macrophage polarization, hinders the mesenchymal transition of fibroblasts and epithelial cells. (A) The $CD11b^+$ cell population in collected BALF was stained for the neutrophil marker, Gr-1, and quantified by FACS analysis. (B) The $F4/80^+$ cell population in collected BALF was stained for the M1 macrophage markers, CD80 and CD86, and analyzed by FACS. (C) $ER\text{-}TR7^+$ and $EPCAM^+$ populations in isolated lung cells were stained for the mesenchymal differentiation marker, vimentin. (D) Relative levels of the cytokines, IL-6, TNF-α, IL-10, and TGF-β, in BALF, analyzed by ELISA. Data are presented as means ± SEM (***$P < 0.001$, **$P < 0.01$, *$P < 0.05$; one-way ANOVA followed by Tukey's post hoc test). BLM, bleomycin-induced pulmonary fibrosis mice.

supported the conclusion that, whereas BRNPs effectively ameliorated the severity of bleomycin-induced pulmonary fibrosis, UCB was totally ineffective and even worsened disease symptoms. This dramatic difference in therapeutic outcomes between BRNPs and UCB may be attributable to their pharmacokinetics and toxicity properties. Unlike UCB, BRNPs can long circulate in the bloodstream (half-life, ~4–6 h) and passively localize in inflamed tissues [13]. Although UCB is metabolized in the liver and excreted from the body under normal condition, in our experimental setting with periodic administration of exogenous UCB, bilirubin may have accumulated to a level that exceeded the metabolic threshold, potentially resulting in various toxicities, such as hemolytic complications [32], as reflected in the poor survival rate of mice in the bleomycin + UCB treatment group (Fig. S5B). To date, however, no such adverse effects have been observed for BRNPs in various mouse models [11–16]. Collectively, these findings indicate that BRNPs are less toxic and constitute a far superior therapeutic compared with native bilirubin.

3.6. BRNPs inhibit neutrophil recruitment and macrophage activation

To examine the mode of action by which BRNPs ameliorate pulmonary fibrosis progression, we first assessed neutrophil recruitment and macrophage activation in collected bronchoalveolar lavage fluid (BALF). Consistent with the observed reductions in pulmonary fibrosis disease indexes, the proportion of neutrophils ($CD11b^{+}Gr\text{-}1^{+}$ cells) in BALF was significantly reduced by BRNP treatment (1.68%) compared with saline treatment (8.05%) (Fig. 6A). Because neutrophils are one of the first immune cells that respond following bleomycin-induced activation of AECs [33–35] and recruited neutrophils produce copious amounts of ROS, thereby resulting in continuous tissue injury [36,37], the attenuation of neutrophil infiltration into the lung suggests that BRNPs mitigated oxidative stress within AECs and prevented the release of neutrophil chemoattractants, confirming results shown in Fig. 2D. Such regulation in the local neutrophil infiltration suggests that BRNPs may play a vital role in obstructing the disease-progression cycle in the early stage of oxidative stress-mediated lung injury, a setting similar to that of SARS-CoV-2 infection.

We next examined whether BRNPs can also influence the activation of macrophages that subsequently release pro-inflammatory cytokines. The degree of macrophage activation in BALF was determined by assessing the M1-phenotype surface markers, CD80 and CD86, by flow cytometry analysis. Compared with normal mice controls, the population of cells expressing high levels of CD80 and CD86 among $F4/80^{+}$ macrophages from the bleomycin+saline group was dramatically increased (5.07% vs. 59.4% for CD80 and 2.96% vs. 33.4% for CD86), whereas BRNPs treatment drastically blunted this increase, significantly reducing CD80 (5.06%) and CD86 levels (17.3%) (Fig. 6B). These results suggest that BRNP treatment suppresses hyper-activation of the pro-inflammatory M1 macrophage phenotype in a model of bleomycin-induced lung injury. On the basis of these findings, we speculate that BRNPs act starting at an early-stage of pulmonary fibrosis progression by reducing bleomycin-induced oxidative damage within AECs and preventing the onset of inflammation by attenuating neutrophil infiltration and macrophage activation.

3.7. BRNPs inhibit the differentiation of fibroblasts and epithelial cells into myofibroblasts

Excessive accumulation of myofibroblasts, a terminal cell type derived from fibroblasts and epithelial cells, is responsible for the expansion of fibrosis and tissue remodeling [38–40]. To assess whether BRNPs affect myofibroblast differentiation, we stained fibroblasts ($ER\text{-}TR7^{+}$) and epithelial cells ($EPCAM^{+}$) from isolated lung homogenates for the mesenchymal filament marker, vimentin. For both cell types, the population of vimentin-expressing cells was increased by ~2-3-fold in the bleomycin + saline treatment group compared with normal controls, an increase that was attenuated (by ~30%) in the bleomycin + BRNPs group (Fig. 6C). Pro-inflammatory and pro-fibrotic mediators are known to drive the differentiation of fibroblasts and epithelial cells into myofibroblasts [41–43]. An analysis of BALF using enzyme-linked immunosorbent assays (ELISAs) revealed that BRNP treatment significantly reduced secretion of the pro-inflammatory cytokines, IL-6 and TNF-α, and pro-fibrotic cytokines, IL-10 and TGF-β (Fig. 6D). Because these mediators are known to be constitutively expressed not only in alveolar macrophages, but also in activated fibroblasts, epithelium, and smooth muscle itself [44], the decrease in these cytokine levels suggests that BRNPs prevented fibrosis-promoting signaling by affecting many different disease-related cell types in wounded pulmonary fibrosis tissue rather than AECs only, consistent with our biodistribution and cellular uptake analyses. Taken together, these findings suggest that BRNPs inhibit the differentiation of fibroblasts and epithelial cells to myofibroblasts, thereby preventing further development of pulmonary fibrosis.

4. Conclusion

Our findings collectively demonstrate that BRNPs have the potential for use as a new therapeutic nanomedicine for the treatment of pulmonary fibrosis. We verified that BRNPs with long blood circulation property and inflamed site-targeting ability are localized in the fibrosis-progressive lung tissue, internalized in phagocytic inflammatory cells and alveolar epithelial cells, thereby reducing the overall ROS levels in the lung and mitigating the disease progression. As illustrated in Fig. S6, we confirmed that scavenging of excess ROS by BRNPs hinders apoptotic signaling and the release of immune cell-infiltrating chemokines. Systemic administration of BRNPs, but not its unmodified counterpart UCB, effectively ameliorated the manifestations of pulmonary fibrosis without notable adverse effects. Additional pathophysiological mechanism studies conducted based on these *in vitro* and *in vivo* findings revealed that BRNP treatment resulted in significantly diminished neutrophil infiltration, macrophage hyper-activation, and differentiation of epithelial cells and fibroblasts into myofibroblasts, in association with reduced collective ROS and disease-related cytokine levels compared with the saline-treated disease group. Although further study is warranted, based on recent clinical evidence that SARS-CoV-2 infection shares similar phenotypic presentations with pulmonary fibrosis, edematous and firm lung parenchyma owing to a redox imbalance resulting from the cellular activities of significantly aggregated neutrophils and inflammatory macrophages [36,45], it is reasonable to speculate that BRNPs could be a feasible therapeutic option for SARS-CoV-2 ARDS. Currently, available medications show limited effectiveness; thus, there is an urgent need for the development of novel, prophylactic anti-fibrotic therapeutics through early intervention. Accordingly, the bilirubin-derived nanomedicine developed herein has potential as a therapeutic option for preventing Covid-19 infection-associated pulmonary fibrosis.

Data availability statement

All data associated with this study are present in the paper or the supplementary materials.

Declaration of competing interest

The authors declare the following financial interests/personal relationships which may be considered as potential competing interests. S. J. declares a financial interest in BiliX. This company did not support the aforementioned research and currently has no rights to any technology or intellectual property developed as part of this research. The rest of the authors declare no competing financial interests.

Acknowledgments

This research was supported by the Basic Science Research Program (Leading Researcher Program: NRF-2018R1A3B1052661), and Global Ph.D. Fellowship Program (NRF-2019H1A2A1074396) through the National Research Foundation of Korea (NRF) funded by the Ministry of Science and ICT. Illustrations on the graphical abstract and figure S6 were created with BioRender.com.

Appendix A. Supplementary data

Supplementary data to this article can be found online at https://doi.org/10.1016/j.biomaterials.2021.120986.

Credit author statement

Hyeongseop Keum: Conceptualization, Investigation, Data curation, Methodology, Writing – original draft, Writing – review & editing; Dohyeon Kim: Methodology; Jinjoo Kim: Methodology; Tae Woo Kim: Methodology; Chang-Hee Whang: Methodology; Wonsik Jung: Methodology; Sangyong Jon: Conceptualization, Formal analysis, Funding acquisition, Project administration, Resources, Supervision, Writing – review & editing

References

[1] A.L. Olson, A.H. Gifford, N. Inase, E.R.F. Perez, T. Suda, The epidemiology of idiopathic pulmonary fibrosis and interstitial lung diseases at risk of a progressive-fibrosing phenotype, Eur. Respir. Rev. 27 (150) (2018).
[2] D.J. Lederer, F.J. Martinez, Idiopathic pulmonary fibrosis, N. Engl. J. Med. 379 (8) (2018) 797–798.
[3] G. Oruqaj, S. Karnati, V. Vijayan, L.K. Kotarkonda, E. Boateng, W.M. Zhang, C. Ruppert, A. Gunther, W. Shi, E. Baumgart-Vogt, Compromised peroxisomes in idiopathic pulmonary fibrosis, a vicious cycle inducing a higher fibrotic response via TGF-beta signaling, P Natl Acad Sci USA 112 (16) (2015) E2048–E2057.
[4] P. Spagnolo, E. Balestro, S. Aliberti, E. Cocconcelli, D. Biondini, G. Della Casa, N. Sverzellati, T.M. Maher, Pulmonary fibrosis secondary to COVID-19: a call to arms? Lancet Resp Med 8 (8) (2020) 750–752.
[5] P.M. George, A.U. Wells, R.G. Jenkins, Pulmonary fibrosis and COVID-19: the potential role for antifibrotic therapy, Lancet Resp Med 8 (8) (2020) 807–815.
[6] P. Cheresh, S.J. Kim, S. Tulasiram, D.W. Kamp, Oxidative stress and pulmonary fibrosis, Bba-Mol Basis Dis 1832 (7) (2013) 1028–1040.
[7] L. Zhang, Y. Wang, G.R. Wu, W.N. Xiong, W.K. Gu, C.Y. Wang, Macrophages: friend or foe in idiopathic pulmonary fibrosis? Respir. Res. 19 (2018).
[8] K.K. Kim, M.R. Dotson, M. Agarwal, J.B. Yang, P.B. Bradley, N. Subbotina, J. J. Osterholzer, T.H. Sisson, Efferocytosis of apoptotic alveolar epithelial cells is sufficient to initiate lung fibrosis, Cell Death Dis. 9 (2018).
[9] A. Nasi, S. McArdle, G. Gaudernack, G. Westman, C. Melief, J. Rockberg, R. Arens, D. Kouretas, J. Sjolin, S. Mangsbo, Reactive oxygen species as an initiator of toxic innate immune responses in retort to SARS-CoV-2 in an ageing population, consider N-acetylcysteine as early therapeutic intervention, Toxicol Rep 7 (2020) 768–771.
[10] M. Laforge, C. Elbim, C. Frere, M. Hemadi, C. Massaad, P. Nuss, J.J. Benoliel, C. Becker, Tissue damage from neutrophil-induced oxidative stress in COVID-19, Nat. Rev. Immunol. 20 (9) (2020) 515–516.
[11] Y. Lee, H. Kim, S. Kang, J. Lee, J. Park, S. Jon, Bilirubin nanoparticles as a nanomedicine for anti-inflammation therapy, Angew. Chem. Int. Ed. 55 (26) (2016) 7460–7463.
[12] J.Y. Kim, D.Y. Lee, S. Kang, W. Miao, H. Kim, Y. Lee, S. Jon, Bilirubin nanoparticle preconditioning protects against hepatic ischemia-reperfusion injury, Biomaterials 133 (2017) 1–10.
[13] D.E. Kim, Y. Lee, M. Kim, S. Lee, S. Jon, S.H. Lee, Bilirubin nanoparticles ameliorate allergic lung inflammation in a mouse model of asthma, Biomaterials 140 (2017) 37–44.
[14] M.J. Kim, Y. Lee, S. Jon, D.Y. Lee, PEGylated bilirubin nanoparticle as an anti-oxidative and anti- inflammatory demulcent in pancreatic islet xenotransplantation, Biomaterials 133 (2017) 242–252.
[15] H. Keum, T.W. Kim, Y. Kim, C. Seo, Y. Son, J. Kim, D. Kim, W. Jung, C.H. Whang, S. Jon, Bilirubin nanomedicine alleviates psoriatic skin inflammation by reducing oxidative stress and suppressing pathogenic signaling, J. Contr. Release 325 (2020) 359–369.
[16] T.W. Kim, Y. Kim, W. Jung, D.E. Kim, H. Keum, Y. Son, S. Jon, Bilirubin nanomedicine ameliorates the progression of experimental autoimmune encephalomyelitis by modulating dendritic cells, J. Contr. Release 331 (2021) 74–84.
[17] A. Allawzi, H. Elajaili, E.F. Redente, E. Nozik-Grayck, Oxidative toxicology of bleomycin: role of the extracellular redox environment, Curr Opin Toxicol 13 (2019) 68–73.
[18] J.E. Chipuk, D.R. Green, Dissecting p53-dependent apoptosis, Cell Death Differ. 13 (6) (2006) 994–1002.
[19] M.T. Hemann, S.W. Lowe, The p53-Bcl-2 connection, Cell Death Differ. 13 (8) (2006) 1256–1259.
[20] L.R. Young, P.M. Gulleman, C.W. Short, H. Tanjore, T. Sherrill, A. Qi, A.P. McBride, R. Zaynagetdinov, J.T. Benjamin, W.E. Lawson, S.V. Novitskiy, T.S. Blackwell, Epithelial-macrophage interactions determine pulmonary fibrosis susceptibility in Hermansky-Pudlak syndrome, Jci Insight 1 (17) (2016).
[21] C.P. Baran, J.M. Opalek, S. McMaken, C.A. Newland, J.M. O'Brien, M.G. Hunter, B. D. Bringardner, M.M. Monick, D.R. Brigstock, P.C. Stromberg, G.W. Hunninghake, C.B. Marsh, Important roles for macrophage colony-stimulating factor, CC chemokine ligand 2, and mononuclear phagocytes in the pathogenesis of pulmonary fibrosis, Am J Resp Crit Care 176 (1) (2007) 78–89.
[22] W.A. Wuyts, C. Agostini, K.M. Antoniou, D. Bouros, R.C. Chambers, V. Cottin, J. J. Egan, B.N. Lambrecht, R. Lories, H. Parfrey, A. Prasse, C. Robalo-Cordeiro, E. Verbeken, J.A. Verschakelen, A.U. Wells, G.M. Verleden, The pathogenesis of pulmonary fibrosis: a moving target, Eur. Respir. J. 41 (5) (2013) 1207–1218.
[23] S. Herold, K. Mayer, J. Lohmeyer, Acute lung injury: how macrophages orchestrate resolution of inflammation and tissue repair, Front. Immunol. 2 (2011).
[24] R. Lester, J.D. Ostrow, R. Schmid, Enterohepatic circulation of bilirubin, Nature 192 (1961) 372.
[25] M.A. Brink, J.F. Slors, Y.C. Keulemans, K.S. Mok, D.R. De Waart, M.C. Carey, A. K. Groen, G.N. Tytgat, Enterohepatic cycling of bilirubin: a putative mechanism for pigment gallstone formation in ileal Crohn's disease, Gastroenterology 116 (6) (1999) 1420–1427.
[26] J.K. Tee, L.X. Yip, E.S. Tan, S. Santitewagun, A. Prasath, P.C. Ke, H.K. Ho, D. T. Leong, Nanoparticles' interactions with vasculature in diseases, Chem. Soc. Rev. 48 (21) (2019) 5381–5407.
[27] G. Burgstaller, B. Oehrle, M. Gerckens, E.S. White, H.B. Schiller, O. Eickelberg, The instructive extracellular matrix of the lung: basic composition and alterations in chronic lung disease, Eur. Respir. J. 50 (1) (2017).
[28] L.C. Li, L. Xu, Y. Hu, W.J. Cui, W.H. Cui, W.C. Zhou, L.D. Kan, Astragaloside IV improves bleomycin-induced pulmonary fibrosis in rats by attenuating extracellular matrix deposition, Front. Pharmacol. 8 (2017).
[29] C.G. Feng, L. Zhang, C. Nguyen, S.N. Vogel, S.E. Goldblum, W.C. Blackwelder, A. S. Cross, Neuraminidase reprograms lung tissue and potentiates lipopolysaccharide-induced acute lung injury in mice, J. Immunol. 191 (9) (2013) 4828–4837.
[30] H. Matsuyama, F. Amaya, S. Hashimoto, H. Ueno, S. Beppu, M. Mizuta, N. Shime, A. Ishizaka, S. Hashimoto, Acute lung inflammation and ventilator-induced lung injury caused by ATP via the P2Y receptors: an experimental study, Respir. Res. 9 (2008).
[31] S. Assaad, W.B. Kratzert, B. Shelley, M.B. Friedman, A. Perrino, Assessment of pulmonary edema: principles and practice, J. Cardiothorac. Vasc. Anesth. 32 (2) (2018) 901–914.
[32] W. Barcellini, B. Fattizzo, Clinical applications of hemolytic markers in the differential diagnosis and management of hemolytic anemia, Dis. Markers 2015 (2015) 635670.
[33] J. Leslie, B.M. Millar, A.D. Pons, R.A. Burgoyne, J.D. Frost, B. Barksby, S. Luli, J. Scott, A.J. Simpson, J. Gauldie, L.A. Murray, D.K. Finch, A.M. Carruthers, J. Ferguson, M.A. Sleeman, D. Rider, R. Howarth, C. Fox, F. Oakley, A.J. Fisher, D. A. Mann, L.A. Borthwick, FPR-1 is an important regulator of neutrophil recruitment and a tissue-specific driver of pulmonary fibrosis, Jci Insight 5 (4) (2020).
[34] A. Pardo, V. Ruiz, J.L. Arreola, R. Ramirez, J. Cisneros-Lira, M. Gaxiola, R. Barrios, S.V. Kala, M.W. Lieberman, M. Selman, Bleomycin-induced pulmonary fibrosis is attenuated in gamma-glutamyl transpeptidase-deficient mice, Am J Resp Crit Care 167 (6) (2003) 925–932.
[35] N.D. Kim, A.D. Luster, The role of tissue resident cells in neutrophil recruitment, Trends Immunol. 36 (9) (2015) 547–555.
[36] M. Laforge, C. Elbim, C. Frere, M. Hemadi, C. Massaad, P. Nuss, J.J. Benoliel, C. Becker, Tissue damage from neutrophil-induced oxidative stress in COVID-19, Nat. Rev. Immunol. 20 (2020) 515–516.
[37] A. van der Vliet, Y.M.W. Janssen-Heininger, V. Anathy, Oxidative stress in chronic lung disease: from mitochondrial dysfunction to dysregulated redox signaling, Mol. Aspect. Med. 63 (2018) 59–69.
[38] L.J. Celada, J.A. Kropski, J.D. Herazo-Maya, W.F. Luo, A. Creecy, A.T. Abad, O. S. Chioma, G. Lee, N.E. Hassell, G.I. Shaginurova, Y.F. Wang, J.E. Johnson, A. Kerrigan, W.R. Mason, R.P. Baughman, G.D. Ayers, G.R. Bernard, D.A. Culver, C. G. Montgomery, T.M. Maher, P.L. Molyneaux, I. Noth, S.E. Mutsaers, C.M. Prele, R. S. Peebles, D.C. Newcomb, N. Kaminski, T.S. Blackwell, L. Van Kaer, W.P. Drake, PD-1 up-regulation on CD4(+) T cells promotes pulmonary fibrosis through STAT3-mediated IL-17A and TGF-beta 1 production, Sci. Transl. Med. 10 (460) (2018).
[39] X.M. Meng, S. Wang, X.R. Huang, C. Yang, J. Xiao, Y. Zhang, K.F. To, D.J. Nikolic-Paterson, H.Y. Lan, Inflammatory macrophages can transdifferentiate into myofibroblasts during renal fibrosis, Cell Death Dis. 7 (2016).
[40] D.H. Kim, J.D. Beckett, V. Nagpal, M.A. Seman-Senderos, R.A. Gould, T.J. Creamer, E.G. MacFarlane, Y.C. Chen, D. Bedja, J.T. Butcher, W. Mitzner, R. Roue, S. Hata, D.S. Warren, H.C. Dietz, Calpain 9 as a therapeutic target in TGF beta-induced mesenchymal transition and fibrosis, Sci. Transl. Med. 11 (501) (2019).
[41] A. van Caam, M. Vonk, F. van den Hoogen, P. van Lent, P. van der Kraan, Unraveling SSc pathophysiology; the myofibroblast, Front. Immunol. 9 (2018).
[42] L.A. Borthwick, T.A. Wynn, A.J. Fisher, Cytokine mediated tissue fibrosis, Bba-Mol Basis Dis 1832 (7) (2013) 1049–1060.

[43] S. Singh, M. Torzewski, Fibroblasts and their pathological functions in the fibrosis of aortic valve sclerosis and atherosclerosis, Biomolecules 9 (9) (2019).
[44] L. Denney, A.J. Byrne, T.J. Shea, J.S. Buckley, J.E. Pease, G.M.F. Herledan, S. A. Walker, L.G. Gregory, C.M. Lloyd, Pulmonary epithelial cell-derived cytokine TGF-beta 1 is a critical cofactor for enhanced innate lymphoid cell function, Immunity 43 (5) (2015) 945–958.
[45] S.E. Fox, A. Akmatbekov, J.L. Harbert, G. Li, J.Q. Brown, R.S. Vander Heide, Pulmonary and cardiac pathology in African American patients with COVID-19: an autopsy series from New Orleans, Lancet Resp Med 8 (7) (2020) 681–686.